Published in final edited form as:
Chem Mater. 2010 August 24; 22(16): 4612–4618. doi:10.1021/cm100657w.

Size and crystallinity in protein-templated inorganic nanoparticles

Craig C. Jolley[1,2], **Masaki Uchida**[1,3], **Courtney Reichhardt**[1], **Richard Harrington**[4], **Sebyung Kang**[1,5], **Michael T. Klem**[1,6], **John B. Parise**[4], and **Trevor Douglas**[1,2,3,*]

[1]Department of Chemistry & Biochemistry, Montana State University

[2]Astrobiology Biogeocatalysis Research Center, Montana State University

[3]Center for Bio-Inspired Nanomaterials, Montana State University

[4]Department of Chemistry and Department of Geosciences, Stony Brook University

Abstract

Protein cages such as ferritins and virus capsids have been used as containers to synthesize a wide variety of protein-templated inorganic nanoparticles. While identification of the inorganic crystal phase has been successful in some cases, very little is known about the detailed nanoscale structure of the inorganic component. We have used pair distribution function analysis of total X-ray scattering to measure the crystalline domain size in nanoparticles of ferrihydrite, γ-Fe_2O_3, Mn_3O_4, CoPt, and FePt grown inside 24-meric ferritin cages from *H. sapiens* and *P. furiosus*. The material properties of these protein-templated nanoparticles are influenced by processes at a variety of length scales: the chemistry of the material determines the precise arrangement of atoms at very short distances, while the interior volume of the protein cage constrains the maximum nanoparticle size attainable. At intermediate length scales, the size of coherent crystalline domains appears to be constrained by the arrangement of crystal nucleation sites on the interior of the cage. Based on these observations, some potential synthetic strategies for the control of crystalline domain size in protein-templated nanoparticles are suggested.

Keywords

Ferritin; Pair Distribution Function; Nanoparticles; Biomineralization

Introduction

In recent years, bio-inspired chemistry has attracted increasing attention as a paradigm for the synthesis of functional nanomaterials[1, 2]. In particular, multimeric protein cages such as virus capsids[3-5], ferritins[6-11], and Dps proteins[12-14] have been used as reaction vessels for the synthesis of protein-templated inorganic nanoparticles and soft branched-polymer structures [15], mimicking the biomolecule-controlled mineralization and hierarchical assembly processes in biomaterials. These protein-templated nanoparticles have several advantages over traditional synthesis methods, particularly the potential for further

*tdouglas@chemistry.montana.edu.
[5]Current address: School of Nano-Biotechnology and Chemical Engineering, Ulsan National Institute of Science and Technology, Ulsan, Korea
[6]Current address: Department of Chemistry, Montana Tech of the University of Montana

Supporting Information Available: Experimental and model PDFs for all samples shown in Figure 3 as well as unmineralized *Pyrococcus* ferritin. Representative unstained TEM images showing nanoparticle cores for various samples.

functionalization through genetic or chemical modifications of the protein cage. Although chemical removal of the protein cage is possible, many desirable features of protein-inorganic nanocomposites depend on leaving it intact and the protein shells were not removed from materials in this study. The protein coating helps passivate particle surfaces and can impart enhanced biocompatibility that makes these materials ideal for *in vivo* applications[16-18], and the ability to generate nanomaterials in aqueous solvent under ambient conditions is an important step forward in the development of green chemistry.

Many of the unique properties of nanomaterials arise from their high surface/volume ratio; as a result, many catalytic nanomaterials show strong size dependence. Catalysis often arises from surface defect sites, and small particles will exhibit a large number of such surface defects, relative to their size. In addition, properties such as magnetic response or bandgap energy are often dependent on the crystalline domain size of a sample. In protein-templated nanoparticle synthesis, the size of nanoparticles can often be controlled by tuning the metal ion/protein cage ratio – this results in a fairly narrow distribution of sizes with a mean value that can be easily controlled during synthesis[19]. The feasibility of technological applications of protein-templated nanoparticles will depend largely on our ability to exert synthetic control over material properties beyond the average particle size, such as the typical crystalline domain size within a nanoparticle. Our results indicate that, in addition to effects arising from the intrinsic material properties of the inorganic phase, the crystalline domain structure of protein-templated nanoparticles is strongly influenced by both the size of the protein cage and (perhaps more importantly) the arrangement of crystal nucleation sites on the cage interior.

As a step toward understanding the role of crystalline domain size in protein-templated nanoparticles, this study uses pair distribution function (PDF) analysis of total X-ray scattering to examine the effects of size and crystallinity in a wide range of protein-templated inorganic materials. Unlike traditional crystallography, which ignores the diffuse (non-Bragg) scattering that contains information about defects and local interactions, PDF analysis involves a Fourier transform of the total scattering over a given range in Q-space, including both the diffuse and Bragg scattering. The pair distribution function, $G(r)$, is effectively a measure of the probability that an observer, located on an average atom within the material, will find another atom located at a displacement of r. $G(r)$ will contain peaks for well-defined atom-atom distances where a neighboring atom is very likely to be found and troughs at intermediate distances where no atom is likely to be found. At distances longer than the average crystalline domain size, $G(r)$ will average out to zero, since it is impossible to find well-defined atom-atom correlations at distances where the lattice periodicity breaks down due to limited crystallinity. The result is that the PDF of nanomaterials tapers off toward zero at a rate that is related to the crystalline domain size; this finite-size effect can be quantified by convoluting the PDF calculated for an ideal infinite lattice with a spherical shape function[20-24]; the diameter of this shape function is a fitting parameter that can be tuned to give optimal agreement between the experimental and calculated $G(r)$. Although the materials under consideration vary in chemical composition and crystal structure, they exhibit common features that can be linked to the process of crystallization in a confined protein cage environment.

Materials & Methods

Ferrihydrite nanoparticle synthesis

Recombinant *Pyrococcus furiosus* ferritin was expressed in *E. coli* BL21 and isolated as described previously[25]. The protein cages and all protein-inorganic composites described below were characterized with size-exclusion chromatography (SEC) and transmission electron microscopy (TEM; LEO 912AB at 100 keV). To synthesize ferrihydrite (Fhyd)

nanoparticles, *P. furiosus* ferritin was diluted to 0.33 mg/mL in 100 mM MOPS, 37.5 mM Na_2SO_4, pH 6.8. A deaerated solution of 12.5 mM $(NH_4)_2Fe(SO_4)_2$ was added at a rate of 5 Fe atoms per ferritin 24-mer per minute using a syringe pump (KD Scientific, Holliston, MA) until the desired loading ratio was reached. The reaction vessel was stirred and left open to the air; no additional oxidant was added. Ferritin-Fhyd composites were synthesized with loading ratios of 250, 500, 750, 1000, 1250, 1500, 1750, 2000, and 2500 Fe/cage. After synthesis, the reaction mixture was concentrated to ~5 mg/mL and purified by SEC on a Superose 6 column. The elution volume of the protein-mineral composite was identical to the elution volume of the empty cages, indicating that mineralization was localized to the inside of the protein cage. As a comparison, native horse spleen ferritin (Calzyme Laboratories), which contains a larger Fhyd core, was also purified by SEC and used for PDF analysis.

Maghemite nanoparticle synthesis

γ-Fe_2O_3 nanoparticles were synthesized in recombinant *H. sapiens* ferritin as described previously[16, 17]. Typically, protein was diluted to a concentration of 1 mg/mL in deaerated 100 mM NaCl. A deaerated 12.5 mM solution of $(NH_4)_2Fe(SO_4)_2$ and a 4.17 mM solution of H_2O_2 were separately added to the reaction vessel at a rate of 158 μL/min (100 Fe/protein cage•min) using a syringe pump. The reaction vessel was maintained at a temperature of 65°C using a water jacket, stirred constantly, and kept under a continuous N_2 flow. A pH of 8.5 was maintained using an autotitrator setup (STAT Titrino, Metrohm) in which 100 mM NaOH was added in order to counteract the release of protons during the hydrolysis of Fe^{2+}. After the reaction mixture had cooled, the mineral-loaded cages were purified by size exclusion chromatography as described above. Ferritin-γ-Fe_2O_3 nanocomposites were synthesized with loading ratios of 200, 400, 1000, 2000, 3000, and 5000 Fe/cage. For comparison, γ-Fe_2O_3 was also synthesized in a protein-free solution under the same temperature and pH conditions; this formed a dark brown precipitate that was strongly attracted to a magnet. Note that γ-Fe_2O_3 (maghemite) and Fe_3O_4 (magnetite) have nearly-identical x-ray PDFs and could not be distinguished in our experiments; we will refer to the protein-templated materials as γ-Fe_2O_3, although the possibility of Fe_3O_4 cannot be excluded.

Mn oxide nanoparticle synthesis

The synthesis of Mn_3O_4 nanoparticles was essentially the same as the γ-Fe_2O_3 nanoparticles described above, except that 12.5 mM $MnCl_2$ was used in place of $(NH_4)_2Fe(SO_4)_2$, with a loading ratio of 1000 Mn/cage. Our procedure differs from the Mn-ferritin syntheses described elsewhere[7, 26], in which Mn oxyhydroxide cores were formed in demineralized horse spleen ferritin by air oxidation at room temperature. A protein-free Mn_3O_4 precipitate was formed in the absence of protein; this was lighter in color than the Fe oxide precipitate and lacked magnetic response.

CoPt nanoparticle synthesis

Ferritin-CoPt nanocomposites were synthesized by a method similar to that described previously for CoPt nanoparticles in demineralized horse spleen ferritin[27, 28] and in the small heat shock protein from *M. jannaschii*[29]. Recombinant *P. furiosus* ferritin was diluted to 1 mg/mL in a buffer containing 50 mM NaCl and 50 mM Tris at pH 8. The temperature in the reaction vessel was maintained at 65°C by flowing water through a jacketed flask. Deaerated 6.25 mM solutions of $Co(NO_3)_2$•$6H_2O$ and K_2PtCl_4 were added at a rate of 0.057 mL/min using a syringe pump until the desired loading of 500 metal atoms/cage was obtained. In order to reduce Co^{2+} and Pt^{2+} to CoPt, 53mM $NaBH_4$ was added to the reaction mixture at the same rate TEM images of stained and unstained CoPt-ferritin nanocomposites

are shown in Figure 1; representative images for the other samples can be found in the Supplementary Information accompanying this article.

FePt nanoparticle synthesis

The synthesis of FePt in ferritin was essentially identical to CoPt, except for the substitution of $(NH_4)_2Fe(SO_4)_2$ for $Co(NO_3)_2 \cdot 6H_2O$.

Pair Distribution Function (PDF) Analysis

Total X-ray scattering was used to determine the crystalline domain size of the ferritin-γ-Fe_2O_3, ferritin-Fhyd, native horse spleen ferritin, ferritin-Mn_3O_4, ferritin-CoPt, and ferritin-FePt nanocomposites. Protein samples were dialyzed against several changes of deionized H_2O over a period of several days to remove salt from the buffer solution and dried to powder using a vacuum lyophilizer (Labconco). X-ray scattering from powdered samples in a cylindrical Kapton capillary (Cole-Parmer) was collected on beamline 11-ID-B at the Advanced Photon Source at Argonne National Laboratories, using a wavelength of 0.2128 Å. Powder diffraction patterns were collected using a Perkin-Elmer amorphous Si area detector and assembled by averaging 1 s exposures, with a total collection time of 2 hours for each sample; the Fit2D software package[30] was used for diffraction image processing. A 1-D trace of the total scattering was obtained by radial integration of the diffraction patterns. The radial pair distribution function $G(r)$ was obtained via a Fourier transform of the corrected X-ray structure factor $S(Q)$; calculation of $S(Q)$ and $G(r)$ used the PDFGetX2 software package[31] with a Q_{max} of 24Å^{-1}. The bulk structural model for Fhyd was based on the structure of bulk Fhyd previously determined by PDF analysis[32], and the bulk structure of all other materials were obtained from the MINCRYST web server[33] or the Inorganic Crystal Structure Database (ICSD)[34]. Crystal models were fit to the experimental $G(r)$ using the PDFgui software package[35]. Uncertainties for fitted parameters (e.g. crystalline domain sizes) were estimated by manually varying the parameter while allowing all others to relax during fitting, and determining the parameter range over which the change in the R-value for the fit was ≤ 5%. This approach yields error estimates that are influenced both by the noise in the data and by parameter correlation during fitting. In order to accurately determine the crystalline domain size, the instrumental damping factor (which causes tapering of $G(r)$ at larger distances than those considered here) was determined using a crystalline Si standard. The determination of crystalline nanodomains by PDF analysis will often give domain sizes that are smaller than the particle sizes seen by electron microscopy, because crystalline nanoparticles are often surrounded by an amorphous boundary phase which does not contribute to the coherent scattering seen in the PDF[36]. Because the present work deals with a comparison of domain sizes from different materials all obtained using the same fitting procedure, systematic differences from other methods will not affect the results.

Results

Crystalline domain size determination from PDF

For each PDF collected, the domain size was determined by fitting a spherical form factor to the amplitude decay of the PDF arising from finite particle size effects. The fitting process assumes spherical domains and, while this assumption is unlikely to be rigorously correct, reliable fits to the experimental $G(r)$ traces were obtained for each sample. Representative $G(r)$ with fits are shown in Figure 2; the complete set of experimental $G(r)$ is available in the online supplementary information.

Figure 3 shows the variation of the observed domain size with metal/cage loading ratio. Several things are immediately apparent from the plotted data. One is that ferritin-γ-Fe_2O_3 synthesis and characterization was possible over a broader range of Fe loading ratios than

ferritin-Fhyd synthesis – at very low Fe loadings the scattering from ferritin-Fhyd was so weak that domain sizes could not be assigned reliably, while at high Fe loadings the ferritin-Fhyd composites aggregated during synthesis and size-exclusion chromatography showed a particle size different from the empty ferritin cages. In the range where their sizes are comparable, however, the γ-Fe_2O_3 samples show larger domain sizes than the Fhyd samples, although even their domain sizes are smaller than γ-Fe_2O_3 synthesized under identical, protein-free conditions (5.4 nm). If the observed domain size is compared to a theoretical maximum particle size based on the loading ratio (Fig. 4), one can see a transition between a regime with very small domains (loading < 1000 Fe/cage) and a regime where the crystalline domains maintain a roughly constant fraction of the theoretical maximum. This suggests that, for nanoparticles larger than 1000 Fe/cage, crystalline domains grow at a roughly uniform rate.

The nearly-constant 2 nm size of the Fhyd domains indicates that the domain size of protein-templated Fhyd is unlikely to grow beyond this point, regardless of the overall particle size. This value is also in good agreement with the domain sizes found in native horse spleen ferritin, which has a Fe loading ratio far higher that what was observed in the protein-templated samples – possibly as high as 4500 Fe/cage[37]. Fhyd synthesized at room temperature has also been shown to have a coherent scattering domain size of around 2 nm[32, 38]; the formation of larger particles requires higher-temperature conditions.

Mineral phase identification for Mn oxide, CoPt and FePt

The Mn oxide nanoparticle PDF data were fit by model PDFs for a variety of Mn oxide phases, including akhtenskite, hausmannite, manganosite, and ramsedellite. The only acceptable fit to the data came from hausmannite (Mn_3O_4), a distorted spinel with a structure similar to magnetite/maghemite. This structural similarity is consistent with the similarity in synthesis conditions between the two materials. A small scattering contribution from bulk NaCl (present in the synthesis buffer and not entirely removed during dialysis) was required to correctly reproduce the PDF at high *r*, and a crystalline domain size of about 35 Å was obtained, somewhat larger than the crystalline domains observed in ferritin-γ-Fe_2O_3 composites. The presence of bulk NaCl meant that scattering at high *r* was dominated by halite peaks; these tended to mask the high-*r* tail of the Mn_3O_4 signal, resulting in an unusually high uncertainty for the particle size – increasing the domain size to 86 Å increased the R-value for the fit by only 5%. Despite this difference in the fitting procedure, the larger domain size in Mn_3O_4 relative to γ-Fe_2O_3 is supported by comparison with the corresponding protein-free materials, in which Mn_3O_4 shows larger nanocrystalline domains of about 17.5 nm, compared to the 5.4 nm observed for γ-Fe_2O_3.

The measured PDF for the FePt/ferritin sample fit to a face-centered cubic (fcc) structure (ICSD #42589). FePt can exist either as a compositionally-disordered fcc phase in which each site is occupied by Fe or Pt with 50% probability, or an ordered face-centered tetragonal (fct) structure, known as the $L1_0$ phase, which contains alternating layers of Fe and Pt. Although the peak locations in the PDFs of these two materials are identical, the relative amplitudes of different peaks in the PDF will differ because of the different scattering lengths of Fe and Pt. The experimental PDF was fit using a model with partial compositional disorder, in which alternating layers contain either Fe with an occupancy of 1-*x* and Pt with an occupancy of *x* or vice versa; $x = 1$ corresponds to the perfectly-ordered case and $x = 0.5$ to the fully disordered case. Fitting in PDFgui converged on an optimal value of $x = 0.82$, suggesting the presence of chemical short-range order[39]. It should be noted, however, that setting *x* to 0.5 or 1.0 increased the R-value of the fit by less than 5%; the X-ray PDF results were insufficient to quantify chemical short-range order at a corresponding level of confidence. Significantly, the 2.0 Å peak arising from Fe-O nearest neighbors in Fe oxides is not visible in the FePt structure, indicating that any contamination

of FePt by Fe oxide phases (which are commonly produced under mild biomimetic conditions) is negligible. The crystalline domain size fit to the FePt data is similar to the domain sizes seen in other ferritin-templated nanoparticles; about 23.5 Å.

The $G(r)$ obtained from the CoPt/ferritin sample gave an excellent fit to a face-centered cubic structure (ICSD #102621). As with FePt, fitting with variable Co/Pt occupancies was used and gave an order parameter of 0.91, but a ≤ 5% increase in the R-value was obtained for order parameters ranging from 0.62-1.0, so the level of short-range order may in fact be quite modest. Protein-templated CoPt nanoparticles in the $L1_0$ phase have previously been synthesized either by thermal annealing[27, 28] (which carbonizes the protein coating) or by the usage of a phage display peptide with an affinity for $L1_0$ CoPt[29]; neither method was employed in the present study and it is not clear to what degree the partial ordering observed was a result of the protein-templated nanoparticle formation. A crystalline domain size of 23.2 Å was observed, similar to FePt.

Relative contributions of protein and inorganic scattering

Close examination of the PDF fits shown in Figure 2 reveals that most protein-inorganic composites include two peaks at short r that are never present in the PDFs calculated from model structures – one peak at about 1.5 Å attributable to the covalent bonds within the protein molecule, and another at 2.5 Å corresponding to second-nearest neighbors either along the peptide backbone or within aliphatic sidechains. These distances can clearly be observed in crystal structures of ferritin[40, 41]; strong 1.5 and 2.5 Å peaks were observed in PDF measurements of lyophilized protein and PDFs calculated from protein crystal structures (see Supplementary Information). As expected, the amplitudes of these protein scattering peaks relative to those arising from the inorganic phase was inversely related to the metal ion loading ratioused during nanoparticle synthesis.

Discussion

There are two major elements at play determining the crystal domain size of protein-encapsulated inorganic minerals. The first is the intrinsic properties of the materials themselves. For example, while the γ-Fe_2O_3 and Fhyd materials grown within ferritin cages are chemically similar, there are important differences in the outcomes of their crystal growth. These are largely foreshadowed by differences in the behavior of the bulk minerals – maghemite can form macroscopic crystals, while Fhyd always exhibits a grain size of 2-6 nm[42]. Mn_3O_4 is formed under the same conditions as γ-Fe_2O_3, but shows a significantly larger crystalline domain size, in agreement with the larger domain sizes of Mn_3O_4 suspensions formed in a protein-free solution – 17.5 nm compared with 5.4 nm for γ-Fe_2O_3. In addition, the size of the protein cage seems to have little influence on the crystallinity of the encapsulated mineral; a previous study [43] gave a crystal domain size of only 18.5 ± 9.5 Å for TiO_2 nanoparticles grown inside the capsid of cowpea chlorotic mottle virus (CCMV). CCMV has an inner diameter of about 20 nm compared to about 8 nm for ferritin; this makes the interior volume of CCMV roughly 16-fold larger than that of ferritin, but the crystalline domain size of TiO_2 in CCMV is actually smaller than some of the ferritin materials examined in this study.

In addition to the undeniable role played by intrinsic material properties, the protein environment also has important effects on nanoparticle structure. This is clearest when comparing the protein-templated samples to corresponding protein-free samples – even the largest γ-Fe_2O_3 and Mn_3O_4 particles show smaller domain sizes than their protein-free counterparts. Some crystal structures of unmineralized ferritin have resolved 24 bound Fe atoms near the ferroxidase active sites. The closest distance between adjacent bound Fe atoms is 26-31 Å; if these are considered to be potential nucleation sites then we can

consider this to be a rough estimate for the maximum diameter to which nascent crystalline domains could grow before beginning to be constrained by their neighbors. The largest crystalline domains measured are only slightly larger than this; growth from multiple adjacent nucleation sites may play a more important role in limiting crystallinity than the confined geometry itself.

Another possibility is that, rather than consisting of a large number of small crystalline domains, our samples simply contain an "amorphous" inorganic phase with a large number of defects, which tend to limit crystalline domain size. If this is the case, then the rough agreement between measured domain sizes and the distances between nucleation sites within the protein cage is simply a fortuitous coincidence; nanoparticle formation could proceed from one or several points within the cage but the growing particles would accumulate defects quickly and the low-temperature synthesis conditions would inhibit the formation of well-ordered crystals. The nanocrystalline interpretation seems somewhat more likely based on the PDFs shown in Figure 2; we would expect glass-like materials to show a broadening of the atom-atom correlations at large values of r due to static positional disorder. Instead, we see a decrease in the amplitude of the PDF peaks (consistent with finite domain sizes) but not substantial broadening. Ultimately, the distinction between amorphous and nanocrystalline materials – if it can be made at all for particles of this size – will depend on the presence of well-defined grain boundaries separating nanocrystalline domains. The direct observation of such grain boundaries is beyond the scope of this study.

These observations place important constraints on the usage of protein-templated inorganic nanoparticles in applications requiring a high degree of crystallinity. Many desirable material features, such as hard ferromagnetism or long charge recombination lengths in photovoltaic materials, depend on the presence of large crystalline domains. If crystallinity in protein-templated nanoparticles is limited by multiple nucleation sites and an apparent lack of Ostwald ripening, then it may be possible to dramatically improve these features by addressing one or both of these features. The presence of multiple nucleation sites, for example, could be addressed by the formation of chimeric particles[44, 45], in which the symmetry of the oligomeric cage is broken and a cage is assembled out of a mixture of two types of subunits, one with and one without crystal nucleation sites. If the concentration of nucleation-competent subunits in the mixture is low enough, growing crystals within a cage will have less competition and may be able to grow to larger sizes without interference from the other subunits. Alternatively, higher-temperature synthesis (enabled by heat-stable protein cages such as *Pyrococcus* ferritin[25]) may be effective in promoting Ostwald ripening that would allow initially independent domains to rearrange into a single crystalline domain.

Further insight into the process of particle growth can be drawn from looking at the γ-Fe_2O_3 particles formed at very low Fe loadings. The domain sizes of the ferritin-γ-Fe_2O_3 composites with 200 and 400 Fe atoms per cage are nearly equal and very small – about 0.5 nm. The PDFs of these samples show only about three peaks, enough to be accounted for by Fe-O clusters of only a few atoms. It appears that the difference between the 200 and 400-Fe composites is the presence of a larger number of these small clusters, and it is at a critical size between 400 and 1000 atoms/cage that larger domains begin to form.

Conclusion

Examination of the crystalline domain size in protein-templated inorganic nanoparticles, as revealed by PDF analysis, can be a useful tool in understanding the process of mineralization inside protein cages. The results presented above indicate that inorganic mineralization in ferritins takes place through the formation of isolated clusters at very low metal loadings; at higher loadings larger domains form. In some materials, such as Fhyd, the

crystalline domain size appears to be limited by inherent properties of the material, largely independent of the presence of the protein cage. In the case of other materials, such as γ-Fe_2O_3 and Mn_3O_4, domain sizes in the protein-templated material are significantly smaller than in material synthesized under protein-free conditions. This suggests that the confined geometry of the protein cage – in particular the presence of multiple nucleation sites – leads to the formation of smaller crystalline domains.

These results also suggest ways in which it might be possible to tune the domain size of inorganic nanoparticles within protein cages. One would be to limit the number of nucleations within an individual cage by mineralizing chimeric cage particles with a smaller number of nucleation sites. Alternatively, one could attempt mineralization at higher temperatures in order to promote the rearrangement of smaller crystallites into a larger growing crystal. By combining higher synthesis temperatures with the superior thermal properties of protein cages from hyperthermophilic organisms such as *P. furiosus*, it may be possible to generate samples with higher degrees of crystallinity and superior material properties.

Supplementary Material

Refer to Web version on PubMed Central for supplementary material.

Acknowledgments

This research was supported in part by a grant from the NASA Astrobiology Institute (NNA08CN85A). CR was supported by grant number P20 RR-16455-08 from the National Center for Research Resources (NCRR), a component of the National Institutes of Health (NIH). RH and JBP acknowledge financial support provided by the National Science Foundation through Collaborative Research in Chemistry (CRC) grant CHE0714183. X-ray scattering was obtained at beamline 11-ID-B at the APS with the assistance of Peter Chupas, Evan Maxey, and Karena Chapman. Use of the Advanced Photon Source was supported by the U.S. Department of Energy, Office of Science, Office of Basic Energy Sciences, under Contract No. DE-AC02-06CH11357. The authors would also like to thank Simon Billinge and Karena Chapman for helpful discussions on the PDF fitting process.

References

1. Dujardin E, Mann S. Bio-inspired materials chemistry. Advanced Materials. 2002; 14(11):775–788.
2. Aizenberg J. Crystallization in patterns: A bio-inspired approach. Advanced Materials. 2004; 16(15):1295–1302.
3. Douglas T, Young M. Viruses: Making friends with old foes. Science. 2006; 312(5775):873–875. [PubMed: 16690856]
4. Young M, Willits D, Uchida M, Douglas T. Plant viruses as biotemplates for materials and their use in nanotechnology. Annual Review of Phytopathology. 2008; 46:361–384.
5. Douglas T, Young M. Host-guest encapsulation of materials by assembled virus protein cages. Nature. 1998; 393(6681):152–155.
6. Douglas T, Dickson DP, Betteridge S, Charnock J, Garner CD, Mann S. Synthesis and Structure of an Iron(III) Sulfide-Ferritin Bioinorganic Nanocomposite. Science. 1995; 269(5220):54–57. [PubMed: 17787702]
7. Meldrum FC, Douglas T, Levi S, Arosio P, Mann S. Reconstitution of Manganese Oxide Cores in Horse Spleen and Recombinant Ferritins. Journal of Inorganic Biochemistry. 1995; 58(1):59–68. [PubMed: 7738539]
8. Wong KKW, Mann S. Biomimetic synthesis of cadmium sulfide-ferritin nanocomposites. Advanced Materials. 1996; 8(11):928. &.
9. Douglas T, Stark VT. Nanophase cobalt oxyhydroxide mineral synthesized within the protein cage of ferritin. Inorganic Chemistry. 2000; 39(8):1828–1830. [PubMed: 12526579]

10. Klem MT, Mosolf J, Young M, Douglas T. Photochemical mineralization of europium, titanium, and iron oxyhydroxide nanoparticies in the ferritin protein cage. Inorganic Chemistry. 2008; 47(7): 2237–2239. [PubMed: 18307300]
11. Klem MT, Young M, Douglas T. Biomimetic synthesis of photoactive alpha-Fe2O3 templated by the hyperthermophilic ferritin from Pyrococus furiosus. Journal of Materials Chemistry. 2010; 20(1):65–67.
12. Ilari A, Latella MC, Ceci P, Ribacchi F, Su M, Giangiacomo L, Stefanini S, Chasteen ND, Chiancone E. The unusual intersubunit ferroxidase center of Listeria innocua Dps is required for hydrogen peroxide detoxification but not for iron uptake. A study with site-specific mutants. Biochemistry. 2005; 44(15):5579–87. [PubMed: 15823016]
13. Bellapadrona G, Stefanini S, Zamparelli C, Theil EC, Chiancone E. Iron translocation into and out of Listeria innocua Dps and size distribution of the protein-enclosed nanomineral are modulated by the electrostatic gradient at the 3-fold “ferritin-like” pores. J Biol Chem. 2009; 284(28):19101–9. [PubMed: 19457858]
14. Kang S, Lucon J, Varpness ZB, Liepold L, Uchida M, Willits D, Young M, Douglas T. Monitoring biomimetic platinum nanocluster formation using mass spectrometry and cluster-dependent H2 production. Angew Chem Int Ed Engl. 2008; 47(41):7845–8. [PubMed: 18767197]
15. Lucon J, Abedin MJ, Uchida M, Liepold L, Jolley CC, Young M, Douglas T. A click chemistry based coordination polymer inside small heat shock protein. Chemical Communications. 2010; 46(2):264–266. [PubMed: 20024346]
16. Uchida M, Flenniken ML, Allen M, Willits DA, Crowley BE, Brumfield S, Willis AF, Jackiw L, Jutila M, Young MJ, Douglas T. Targeting of cancer cells with ferrimagnetic ferritin cage nanoparticles. J Am Chem Soc. 2006; 128(51):16626–33. [PubMed: 17177411]
17. Uchida M, Terashima M, Cunningham CH, Suzuki Y, Willits DA, Willis AF, Yang PC, Tsao PS, McConnell MV, Young MJ, Douglas T. A human ferritin iron oxide nano-composite magnetic resonance contrast agent. Magn Reson Med. 2008; 60(5):1073–81. [PubMed: 18956458]
18. Uchida M, Willits DA, Muller K, Willis AF, Jackiw L, Jutila M, Young MJ, Porter AE, Douglas T. Intracellular Distribution of Macrophage Targeting Ferritin-Iron Oxide Nanocomposite. Advanced Materials. 2009; 21(4):458. +
19. Kang S, Jolley CC, Liepold LO, Young M, Douglas T. From metal binding to nanoparticle formation: monitoring biomimetic iron oxide synthesis within protein cages using mass spectrometry. Angew Chem Int Ed Engl. 2009; 48(26):4772–6. [PubMed: 19455534]
20. Mason G. Radial Distribution Functions from Small Packings of Spheres. Nature. 1968; 217(5130):733. &.
21. Gilbert B, Huang F, Zhang HZ, Waychunas GA, Banfield JF. Nanoparticles: Strained and stiff. Science. 2004; 305(5684):651–654. [PubMed: 15232073]
22. Qiu XY, Proffen T, Mitchell JF, Billinge SJL. Orbital correlations in the pseudocubic O and rhombohedral R phases of LaMnO3. Physical Review Letters. 2005; 94(17)
23. Kodama K, Iikubo S, Taguchi T, Shamoto S. Finite size effects of nanoparticles on the atomic pair distribution functions. Acta Crystallographica Section A. 2006; 62:444–453.
24. Lei M, de Graff AMR, Thorpe MF, Wells SA, Sartbaeva A. Uncovering the intrinsic geometry from the atomic pair distribution function of nanomaterials. Physical Review B. 2009; 80(2)
25. Parker MJ, Allen MA, Ramsay B, Klem MT, Young M, Douglas T. Expanding the temperature range of biomimetic synthesis using a ferritin from the hyperthermophile Pyrococcus furiosus. Chemistry of Materials. 2008; 20(4):1541–1547.
26. Meldrum FC, Wade VJ, Nimmo DL, Heywood BR, Mann S. Synthesis of Inorganic Nanophase Materials in Supramolecular Protein Cages. Nature. 1991; 349(6311):684–687.
27. Warne B, Kasyutich OI, Mayes EL, Wiggins JAL, Wong KKW. Self assembled nanoparticulate Co : Pt for data storage applications. Ieee Transactions on Magnetics. 2000; 36(5):3009–3011.
28. Mayes E, Bewick A, Gleeson D, Hoinville J, Jones R, Kasyutich O, Nartowski A, Warne B, Wiggins J, Wong KKW. Biologically derived nanomagnets in self-organized patterned media. Ieee Transactions on Magnetics. 2003; 39(2):624–627.
29. Klem MT, Willits D, Solis DJ, Belcher AM, Young M, Douglas T. Bio-inspired synthesis of protein-encapsulated CoPt nanoparticles. Advanced Functional Materials. 2005; 15(9):1489–1494.

30. Hammersley AP, Svensson SO, Hanfland M, Fitch AN, Hausermann D. Two-dimensional detector software: From real detector to idealised image or two-theta scan. High Pressure Research. 1996; 14(4-6):235–248.

31. Qiu X, Thompson JW, Billinge SJL. PDFgetX2: a GUI-driven program to obtain the pair distribution function from X-ray powder diffraction data. Journal of Applied Crystallography. 2004; 37(4):678.

32. Michel FM, Ehm L, Antao SM, Lee PL, Chupas PJ, Liu G, Strongin DR, Schoonen MAA, Phillips BL, Parise JB. The structure of ferrihydrite, a nanocrystalline material. Science. 2007; 316(5832): 1726–1729. [PubMed: 17525301]

33. Chichagov AV, Varlamov DA, Dilanyan RA, Dokina TN, Drozhzhina NA, Samokhvalova OL, Ushakovskaya TV. MINCRYST: a crystallographic database for minerals, local and network (WWW) versions. Crystallography Reports. 2001; 46(5):876–879.

34. Belsky A, Hellenbrandt M, Karen VL, Luksch P. New developments in the Inorganic Crystal Structure Database (ICSD): accessibility in support of materials research and design. Acta Crystallographica Section B-Structural Science. 2002; 58:364–369.

35. Farrow CL, Juhas P, Liu JW, Bryndin D, Bozin ES, Bloch J, Proffen T, Billinge SJL. PDFfit2 and PDFgui: computer programs for studying nanostructure in crystals. Journal of Physics-Condensed Matter. 2007; 19(33)

36. Zhang HZ, Chen B, Banfield JF, Waychunas GA. Atomic structure of nanometer-sized amorphous TiO2. Physical Review B. 2008; 78(21)

37. Liu X, Theil EC. Ferritins: dynamic management of biological iron and oxygen chemistry. Acc Chem Res. 2005; 38(3):167–75. [PubMed: 15766235]

38. Cornell, RM.; Schwertmann, U. The iron oxides : structure, properties, reactions, occurrences, and uses. 2nd, completely rev. and extended ed. Wiley-VCH; Weinheim: 2003. p. 664

39. Proffen T, Petkov V, Billinge SJL, Vogt T. Chemical short range order obtained from the atomic pair distribution function. Zeitschrift Fur Kristallographie. 2002; 217(2):47–50.

40. Langlois d'Estaintot B, Santambrogio P, Granier T, Gallois B, Chevalier JM, Precigoux G, Levi S, Arosio P. Crystal structure and biochemical properties of the human mitochondrial ferritin and its mutant Ser144Ala. J Mol Biol. 2004; 340(2):277–93. [PubMed: 15201052]

41. Tatur J, Hagen WR, Matias PM. Crystal structure of the ferritin from the hyperthermophilic archaeal anaerobe Pyrococcus furiosus. J Biol Inorg Chem. 2007; 12(5):615–30. [PubMed: 17541801]

42. Michel FM, Ehm L, Liu G, Han WQ, Antao SM, Chupas PJ, Lee PL, Knorr K, Eulert H, Kim J, Grey CP, Celestian AJ, Gillow J, Schoonen MAA, Strongin DR, Parise JB. Similarities in 2-and 6-line ferrihydrite based on pair distribution function analysis of X-ray total scattering. Chemistry of Materials. 2007; 19(6):1489–1496.

43. Jolley, CC.; Klem, MT.; Harrington, R.; Parise, JB.; Douglas, T. Structure and photoactivity of a virus capsid-TiO_2 nanocomposite. 2010. Submitted

44. Kang S, Oltrogge LM, Broomell CC, Liepold LO, Prevelige PE, Young M, Douglas T. Controlled assembly of bifunctional chimeric protein cages and composition analysis using noncovalent mass spectrometry. J Am Chem Soc. 2008; 130(49):16527–9. [PubMed: 19554690]

45. Kang S, Suci PA, Broomell CC, Iwahori K, Kobayashi M, Yamashita I, Young M, Douglas T. Janus-like Protein Cages. Spatially Controlled Dual-Functional Surface Modifications of Protein Cages. Nano Letters. 2009; 9(6):2360–2366. [PubMed: 19441792]

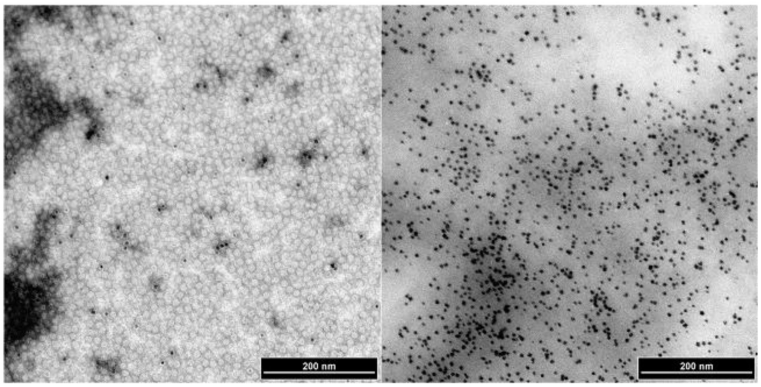

Figure 1.
TEM images of CoPt-ferritin nanocomposites, with (left) and without (right) uranyl acetate staining. The stained image shows the protein cages, while only the inorganic nanoparticles can be seen in the unstained image.

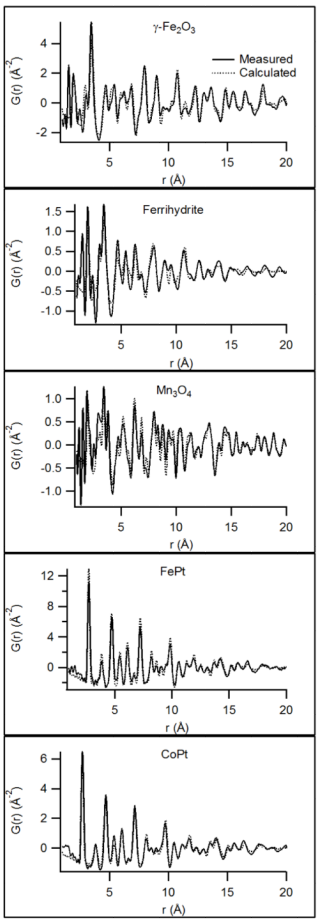

Figure 2.

Representative PDFs with theoretical fits. Note the more rapid tapering of G(r) in the lesscrystalline samples (especially Fhyd) relative to the more-crystalline γ-Fe_2O_3 and Mn_3O_4. Most samples show protein scattering peaks at ~1.5 Å and ~2.5 Å that are not reproduced in the model fits; their absence in FePt and CoPt can be attributed to the very strong X-ray scattering from electron-rich Pt that completely overwhelms the protein scattering.

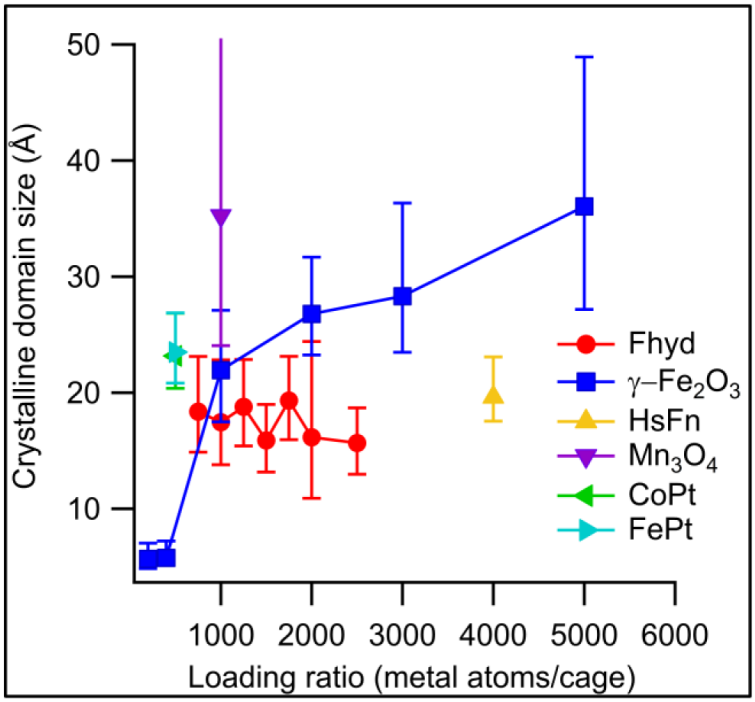

Figure 3.

Domain sizes in ferritin-templated inorganic nanoparticles. The most-crystalline materials are Fe_3O_4 and Mn_3O_4, while Fhyd shows lower crystallinity. Native horse spleen ferritin (HsFn) is fit with a calculated PDF from ferrihydrite and shows a domain size similar to much smaller ferrihydrite particles. The error bar for Mn_3O_4 is off the scale for this image; see text for discussion.

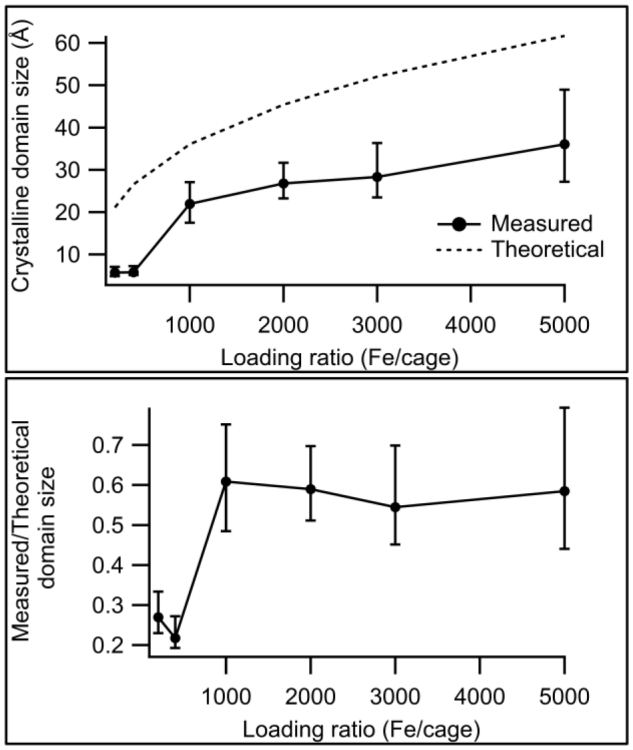

Figure 4.

Comparison of measured and theoretical (single-crystal) domain sizes in ferritin-Fe_3O_4 nanoparticles. Note the transition between the regime of very small domains (at 200 and 400-Fe loadings) and the regime where the observed domain size is roughly proportional to the theoretical maximum domain size (≥ 1000 Fe/cage).